Article

Not peer-reviewed version

Hydrological Modeling in the Upper Lancang-Mekong River Basin Using Global and Regional Gridded Meteorological Reanalyses

Shixiao Zhang , Yang Lang * , Furong Yang , Xinran Qiao , Xiuni Li , Yuefei Gu , Qi Yi , Lifeng Luo , Qingyun Duan

Posted Date: 26 April 2023

doi: 10.20944/preprints202304.0983.v1

Keywords: CMADS; CFSR; meteorological variables; hydrological simulations; SWAT+; upper Lancang-Mekong River Basin

Article

Hydrological modeling in the upper Lancang-Mekong River Basin using global and regional gridded meteorological reanalyses

Shixiao Zhang [1], Yang Lang [1,*], Furong Yang [1], Xinran Qiao [1], Xiuni Li [1], Yuefei Gu [2], Qi Yi [1], Lifeng Luo [3,4] and Qingyun Duan [5]

[1] School of Earth Science, Yunnan University, Kunming 650050, P. R. China; zhangsx_98@163.com (S.Z.); 18008349012@163.com (F.Y.); a1260019225@163.com (X.Q.); lxn6471@mails.ccnu.edu.cn (X.L.); yiqi@ynu.edu.cn (Q.Y.)
[2] Institute of International Rivers and Eco-security, Yunnan University, Kunming 650050, P. R. China; gyfszjs@163.com (Y.G.)
[3] Department of Geography, Environment, and Spatial Sciences, Michigan State University, East Lansing, MI 48824, USA; lluo@msu.edu (L.L.)
[4] Center for Global Change and Earth Observations, Michigan State University, East Lansing, MI 48824, USA
[5] College of Hydrology and Water resources, Hohai University, Nanjing 210098, P. R. China; qyduan@hhu.edu.cn (Q.D.)
* Correspondence: langyang@ynu.edu.cn

Abstract: Multisource meteorological re-analyses are the most reliable forcing data for driving hydrological models to simulate streamflow. We aimed to assess the different hydrological responses through hydrological modeling in the upper Lancang-Mekong River Basin (LMRB) using the two gridded meteorological datasets, climate forecast system reanalysis (CFSR) and the China Meteorological Assimilation Driving Datasets for the SWAT model (CMADS). We selected the Pearson's correlation coefficient (R), percent bias (PBIAS), and root mean square error (RMSE) indices to compare the six meteorological variables of the two datasets. The spatial distributions of the statistical indicators in the CFSR and CMADS, namely, the R, PBIAS, and RMSE values, were different. Furthermore, the soil and water assessment tool plus (SWAT+) model was used to do hydrological modeling based on CFSR and CMADS meteorological re-analyses in the upper LMRB. Different meteorological datasets resulted in significant differences of hydrological responses, which reflected by different sensitive parameters and their optimal value. These different calibrated optimal values of sensitive parameters further lead to the different simulated water balance components between CFSR- and CMADS-based SWAT+ model. These findings can help in a better understanding of the strengths and weaknesses of different meteorological re-analysis datasets and the roles on the hydrological modeling.

Keywords: CFSR; CMADS; meteorological variables; hydrological simulations; SWAT+; upper Lancang-Mekong River Basin (LMRB)

1. Introduction

Both climate change and anthropogenic activities influence the changes in streamflow [1]. While there are no clear trends of changing streamflow at the global level, they do exist at a regional level. As one of the longitudinal large mountainous watersheds, the LMRB has shown sensitivity to the impacts of climate change [2] and socio-economic activities and agricultural production. In the past few decades, annual streamflow in the LMRB has shown no significant trends and is in a state of normal fluctuation [3]. However, greater variability in runoff is expected due to climate change [4] and anthropogenic activities [5]. Moreover, studies based on climate projections from general circulation models have reported that streamflow in the Lancang-Mekong River will increase significantly due to climate change [6,7], leading to an increased risk of flooding [8,9]. In order to better understand the changes in hydrological conditions and strengthen the water resource management and impact assessment of LMRB, relatively accurate hydrological simulation or

hydrological modeling is necessary [10]. Reanalysis datasets are reliable forcing inputs for hydrological simulations as they can be used to compensate for the in situ observations in the LMRB [10,11]. A review of climate proxies indicated that re-analyses have a large number of climate variables that can be easily used for streamflow simulations [12]. However, there are significant biases in the different re-analyses due to a variety of data sources, assimilation techniques, and model equations [13]. Different meteorological forcing reanalysis products provide us with the opportunity to understand the differences between re-analyses and how they behave during hydrological modeling in the LMRB.

In order to investigate the potential applicability of meteorological forcing re-analyses on hydrological simulation or prediction, several studies have evaluated meteorological forcing re-analyses following one of two procedures: (1) comparison of re-analysis products with the corresponding observations on spatiotemporal scales [10,13–16]; or (2) comparison of the meteorological forcing re-analyses based simulated streamflows with the hydrological observations [10,11,14–17]. Several studies have compared the precipitation and temperature of global atmospheric re-analyses with the gridded-observed data [10,13]. They compared precipitation and temperature from various global and regional meteorological re-analyses with gridded observations, and found that there are large differences between the re-analyses and the gridded observations. The temperature of CFSR was more realistic than its precipitation, while the precipitation of the CFSR is higher than that in the observed data. Owing to the sparse and discontinuous meteorological data from East Asia, CMADS was developed to provide regional gridded meteorological re-analyses [18]. With the wide application of CMADS in East Asia [19], many studies compared the meteorological variables of CFSR and CMADS with the observed data [14–16,20]. Gao et al. [14] and Wang et al. [20] evaluated the performance of CMADS and CFSR with gauge observations on two time steps (daily and monthly). They found that CFSR tends to overestimate the precipitation, while CMADS tends to underestimate it on both time steps. CMADS exhibits a greater accuracy in detecting precipitation events [20]. Two studies evaluated CMADS and CFSR in different regions of China [16]. Liu et al. [15] found that the performance of precipitation in CFSR and CMADS was poor and CFSR precipitation was overestimated in the Qinghai-Tibet Plateau, while Zhang et al. [16] found that the performance of precipitation in CFSR and CMADS was good in Northeast China. They all found that the performance of max/min temperature was good, but CFSR temperatures were underestimated. The performance of humidity and wind speed in the CFSR was inferior to that in the CMADS, with low correlation and high bias [15].

The differences in meteorological forcing re-analyses can lead to different hydrological responses, due to the fact that the errors in meteorological inputs can be propagated through the hydrological models into runoff simulations [21,22], such as parameter sensitivity and optimization [23,24]. Dile and Srinivasan [17] applied conventional weather observed data and CFSR data in the uncalibrated SWAT model, to compare the CFSR-based streamflow simulation with the traditional weather-based streamflow simulation in monthly time steps. And the results demonstrated that the CFSR-based streamflow simulation had a lower performance rate than did the conventional weather-based streamflow simulation, and the CFSR-based streamflow simulation substantially underestimated streamflow. The water balance components in two streamflow simulation are similar, but the contribution of surface streamflow and base flow to total streamflow are different. Fuka et al. [11] evaluated the simulated streamflows of CFSR data and conventional weather station data on a daily time step. They performed separate the SWAT model calibrations for each meteorological dataset, and all the results showed that CFSR-based streamflow simulation is as good as, or better than, the conventional weather-based streamflow simulation. They speculated that the advantage is that the CFSR data represent a watershed area better than does a weather station. Lauri et al. [10] assessed the daily streamflow simulation driven by global and regional gridded temperature and precipitation datasets in the Mekong River basin. The results demonstrated that the CFSR-based streamflow simulation had a lower performance rate than did the remotely sensed precipitation-based streamflow simulation. CFSR and CMADS, freely available global and regional gridded meteorological re-analyses, contain six consistent meteorological elements. These

meteorological elements satisfy the operation of the SWAT model. Gao et al. [14] assessed the performance of precipitation data from CMADS and CFSR, as drivers for streamflow simulations, and used separate SWAT model calibrations for each meteorological dataset to ensure a relatively accurate streamflow simulation. The results demonstrated that the CFSR precipitation-based streamflow simulation had a much lower performance rate than did CMADS. They concluded that the poor performance of CFSR in streamflow simulation was because CFSR overestimates precipitation. However, Wang et al. [20] assessed streamflow simulations based on CFSR precipitation and CMADS precipitation with gauge-observed precipitation-based streamflow, the SWAT model was calibrated by gauge-observed meteorological elements. They found that CFSR precipitation-based streamflow simulation are inferior. Liu et al. [15] and Zhang et al. [16] compared CFSR-based streamflow simulation in relation to CMADS-based streamflow simulation on daily and monthly time steps. They performed separate SWAT model calibrations for each meteorological dataset. The results demonstrated that the CFSR-based streamflow simulation had a lower performance rate than did CMADS-based streamflow simulation. An unexpected finding was that the performance of traditional weather gauging station-based streamflow simulation is unsatisfactory [15], but the reasons were not explained further. However, previous studies focused mainly on evaluation of the streamflow simulation, without fully describing the different hydrological responses.

Our study aimed to validate the applicability of the re-analysis datasets and to assess different hydrological responses in the SWAT+ model simulations. In addition to the analysis of important meteorological variables, such as precipitation and temperature, as conducted in previous studies, we analyzed other meteorological variables of the re-analysis datasets, including relative humidity, wind speed, and solar radiation. The spatiotemporal characteristics of these meteorological variables were validated for the period 2008–2013. We used the newly developed SWAT+ hydrological model and SWAT+ parameters sensitivity/optimization toolbox and algorithms to present the different hydrological responses based on the different meteorological re-analysis datasets in the upper LMRB. The findings can help in a better understanding of the roles of meteorological re-analysis datasets and hydrological model structure in hydrological process.

2. Materials and Methods

2.1. Study Area

The upper Lancang-Mekong River is one of the main rivers located in southwest China and is the most typical north-south river in the world (Figure 1), with a length of approximately 2129 km and a drainage area of 1.87×105 km^2. The LMRB spans the tropical, subtropical, and temperate climate zones, and possesses unique hydrological characteristics, owing to its great regional variety. Due to the monsoon, the upper LMRB is dry and cold in winter and hot and humid in summer, and the annual precipitation in the region is distributed unevenly. The precipitation in the wet season in the LMRB accounts for the majority of the annual precipitation, and the seasonal changes are significant. Therefore, floods and droughts are the major natural disasters in the upper LMRB. According to statistical data acquired from the Yunnan Water Resources Department (http://wcb.yn.gov.cn/html/shuiziyuangongbao/), the average recurrence of floods in the upper LMRB is 9 years for major floods and 3 years for minor ones, and most floods occur between June and August. The average flooding frequency in this region is 3–5 years. These natural disasters have caused huge losses to agriculture in the downstream areas of Mekong river, which include several developing countries. All these countries are highly dependent on agriculture, fishing, and hydropower; therefore, the forecasting, governance, and management of floods and droughts in these areas are extremely important.

Preprints (www.preprints.org) | NOT PEER-REVIEWED | Posted: 26 April 2023 doi:10.20944/preprints202304.0983.v1

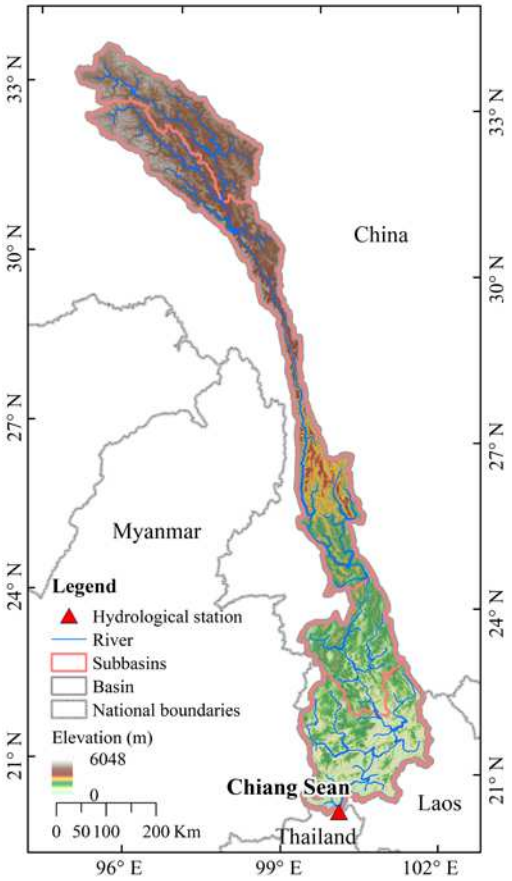

Figure 1. DEMs, delineated watershed, and location of the Chiang Sean hydrological station over the upper LMRB.

2.2. Data

The NCEP CFSR is a new generation of reanalysis product, which provided the best estimate of the land surface state from 1979 to 2014 and developed from the global high-resolution atmosphere-ocean-land surface-sea ice coupling system and data assimilation system [25]. Notably, the CFSR datasets have a global high resolution (T382L64). The CFSR datasets provide six meteorological variables for hydrological model, including precipitation, maximum/minimum temperatures, relative humidity, wind speed, and solar radiation. We downloaded daily meteorological variables in the SWAT file format from the SWAT data website (https://swat.tamu.edu/data/cfsr). In order to perform grid-to-grid comparison between CFSR and CMADS meteorological re-analyses, the coordinates of CFSR were interpolated to those of CMADS by bilinear interpolation method.

Different from the global reanalysis datasets CFSR, CMADS is a regional reanalysis data developed by Dr. Meng Xianyong, mainly covering East Asia (0 ° -65 ° N, 60 ° -160 ° E). The CMADS product was constructed through assimilation and correction of the meteorological observation (automatic stations, satellites, and radars) and the European Centre for Medium-Range Weather Forecasts background field using multiple technologies and scientific methods, including resampling, bilinear interpolation, and the loop nesting of data [26]. The assimilation process of CMADS is mainly achieved through LAPS and STMAS system. CMADS is available to the public, which is benefited for the areas in East Asia, especially for the regions with relatively scarce meteorological data. In this study, we used CMADS version 1.0 (1/3 °), which is freely available (http://www.cmads.org/). We chose the 6-year common period (i.e., 2008–2013), to evaluate the meteorological datasets of the CFSR for the upper LMRB.

In addition to meteorological forcings, other land surface data are needed for delineating the watershed, including DEMs, land use, and soil type. The 90 meter DEM were acquired from the

Preprints (www.preprints.org) | NOT PEER-REVIEWED | Posted: 26 April 2023 doi:10.20944/preprints202304.0983.v1

National Aeronautics and Space Administration and the Department of Defense's National Imagery and Mapping Agency. The land use data were obtained from the Earth Resources Observation and Science Center, which adopts USGS LULC 24 classification standard. The soil type data were required from the Food and Agriculture Organization of the United Nations [27], which was published in 2003 (https://www.fao.org). The gauged streamflow at the Chiang Sean hydrological station, obtained from the Mekong River commission.

There are eight main LULC types in the upper LMRB (Table.S1), including grassland, mixed forest, evergreen broad-leaved forest, tundra, savanna, deciduous broad-leaved forest, shrub land and irrigated farmland and pasture. The coverage area of grasslands and mixed forests exceeds half of the total watershed area, and are mainly distributed in the upstream and downstream regions, respectively. There are 11 identified soil types and two dominant soil textures (loam and sandy_clay_loam) in the upper LMRB (Table.S2). More information on soil type are listed in Table S2 of the supplementary materials. Based on these geographical data, the upper LMRB were delineated to achieve a stream network based on QGIS Interface for SWAT+ 2.0. We created four subbasins from the DEM by specifying area thresholds and outlet. To ensure accurate Landscape unit of HRUs to separate floodplain and upslope areas, we created 110 landscape units by demarcating the floodplain simply as a buffer drawn around the stream reaches. For each landscape unit, the largest potential HRUs was chosen to be the dominant HRU, sharing the same land use, soil, and slope range [28]. Streamflow was generated from each HRU separately and then determine the route to obtain the total streamflow for the watershed, which provided a much better physical description of the water balance [29,30].

2.3. Evaluation Index

The performance of the CFSR meteorological datasets was evaluated for the 6-year common period (2008–2013), using R, PBIAS, and RMSE. R was used to measure the correlation between the variables of CFSR and CMADS; if the R value was close to 1, the two variables were considered to be linearly related. Furthermore, PBIAS in this study is a measure of the average trend of CFSR greater than or less than CMADS [31,32]. The optimal PBIAS value was considered as 0 (%). Low absolute values indicated an accurate model simulation, such as a good model performance could be ±25 %. A positive value of PBIAS indicated an overestimation (by the model), whereas a negative value indicated an underestimation. Finally, the RMSE was used for measuring the differences between values predicted by the model and the observed values, a smaller value indicating better model performance.

$$R=\frac{\sum(X_t-\bar{X})(Y_t-\bar{Y})}{\sqrt{\sum(X_t-\bar{X})^2}\sqrt{\sum(Y_t-\bar{Y})^2}}, \quad (1)$$

$$PBIAS=\frac{\sum(X_t-Y_t)\times 100}{\sum Y_t}, \quad (2)$$

$$RMSE=\sqrt{\frac{1}{N}\sum(X_t-Y_t)^2}, \quad (3)$$

where X_t indicates the meteorological variables of the CFSR datasets, Y_t indicates the meteorological variables of the CMADS datasets, including six mereological elements, and $\bar{X}$ and $\bar{Y}$ indicate the average values of the CFSR and CMADS meteorological variables, respectively.

The Nash-Sutcliffe efficiency coefficient (NSE), coefficient of determination (R^2), and PBIAS were used to evaluate the hydrological model simulations based on the CFSR and CMADS meteorological datasets, respectively, for the 6-year common period (2008–2013). The NSE reflects the degree of fit between the simulated and observed streamflow [33]. If NSE approaches 1, it indicates the most accurate hydrological simulation. Moriasi et al. [34] recommended the use of performance ratings to measure the SWAT performance. For the monthly time step, 0.75 < NSE < 1 and PBIAS < ±10 % indicated that the hydrological simulations were very good. The values of 0.65 < NSE < 0.75, and ±10 % ≤PBIAS ≤ ± 15 % indicated that hydrological simulations were good; 0.50 < NSE < 0.65 and ± 15

Preprints (www.preprints.org) | NOT PEER-REVIEWED | Posted: 26 April 2023 doi:10.20944/preprints202304.0983.v1

%≤ PBIAS ≤± 25 % indicated that the hydrological simulations were satisfactory; while NSE ≤0.5 and PBIAS ≥ ± 25 % indicated that the hydrological simulations were unsatisfactory. Note that R^2 was used to measure the accuracy of the simulated streamflow. The equations used to calculate the statistical indexes are shown below:

$$NSE=1-\frac{\Sigma (Q_o^t-Q_m^t)^2}{\Sigma (Q_o^t-\overline{Q_o^t})^2}, \quad (4)$$

$$R^2=\frac{(\Sigma (Q_o^t-\overline{Q_o^t})\Sigma (Q_m^t-\overline{Q_m^t}))^2}{\Sigma (Q_o^t-\overline{Q_o^t})^2 \Sigma (Q_m^t-\overline{Q_m^t})^2}, \quad (5)$$

$$PBIAS=\frac{\Sigma (Q_m^t-Q_o^t)\times 100}{\Sigma Q_o^t}, \quad (6)$$

where Q_o^t, Q_m^t, $\overline{Q_o^t}$, $\overline{Q_m^t}$ denote the observed, simulated, observed average, and simulated average streamflows at time t, respectively.

2.4. Hydrological Models

The SWAT model aims to predict the long-term effects of land management practices on the production of water, sediment and agricultural chemicals in large complex watersheds with different soil, land use and management conditions [30]. Note that the SWAT+ is a completely restructured version of the SWAT. As a semi-distribution hydrological model, the SWAT+ can effectively simulate the flow and pollutant transport of rivers under different conditions and scenarios across a wide range of spatiotemporal scales. Bieger et al. [29] concluded that the SWAT+ model is more flexible in terms of the delineation and interaction of the spatial objects in a watershed, while offering users the opportunity to achieve a more realistic spatial representation of their target watershed areas.

In this study, we used a new and free SWAT+ model version 2.0.6 to do the hydrological modeling in the upper LMRB based on QSWAT+ platform, which is the Quantum GIS 3.16 Interface for SWAT+. The SWAT+ model provides diverse options of physical processes at watershed level. Driving SWAT+ model, we used the Penman/Monteith method, the Soil Conservation Service's curve number method and the variable storage routing method to calculate PET, estimate surface runoff and determine the route of streamflow in the channel respectively.

2.5. SWAT+ Parameter Sensitivity Analysis and Calibration Tool

In our study, we used a new and free SWAT+ Toolbox v1.0 to carry out the parameter sensitivity analysis (SA), as well as calibration and validation, for the upper LMRB. Sobol' method, an available quantitative SA method in the SWAT+ Toolbox, was used in this study for the upper LMRB, which can indicate the degree of sensitivity of the parameters according to the contributions of each parameter to the final output results [35,36]. SA is the identification of parameters that are sensitive to the hydrological processes in different study areas [37,38]. Based on several studies [35,39,40], we considered 24 commonly used parameters, along with their previously established reference ranges, for the parameter sensitivity analysis. For Sobol's quantitative SA, we specify 100 seed for each parameter, then 5000 samples were randomly generated from 24 tunable parameter ranges [41,42]. We can obtain the 1st order sensitivity results of each parameter after 5000 times SWAT+ model simulation run. The sensitivities of the parameters were ranked by the absolute value of the 1st order sensitivity. After determining the model-sensitive parameters, we calibrated the sensitive parameters, using the observed streamflow obtained from Chiang Sean station, as reference. In order to represent the realistic physical process in the SWAT+ model, we use calibration procedure to improve the fitting degree between simulated streamflow and observed streamflow [43]. The SWAT+ Toolbox provides an available dynamically dimensioned search (DDS) automatic calibration algorithm [44], which can automatically expand the search to find a good solution without tuning algorithm parameter. The DDS automatic calibration algorithm have an outstanding performance in both convergence speed and parameter sets searching ability [45,46]. Finally, we validated the

 doi:10.20944/preprints202304.0983.v1

optimal parameter value of the SWAT+ model for the streamflow simulation. According to the time length of meteorological datasets and the observed streamflow from the Chiang Saen Station, we chose 2008 as the warming-up period, 2009–2010 as the calibration period, and 2011–2013 as the validation period.

3. Results

3.1. Spatial Annual Average Distribution of CFSR Dataset and the Difference for LMRB

We evaluated six meteorological variables of the CFSR dataset using a multi-source meteorological dataset (CMADS). For grid-to-grid comparisons, we consistently interpolated the spatial resolution of the two datasets to 0.3°. The difference maps were computed by subtracting the average annual meteorological variables of the CMADS dataset from the average annual values of CFSR dataset. Figure 2 portrays the annual average of the six meteorological variables from 2008–2013 and the differences between the average annual values of the CFSR and CMADS datasets. The spatial distributions of the annual mean precipitation values of these two datasets were highly similar, indicating less precipitation in the northwest region and more precipitation in the southeast region. However, the average annual precipitation of the CFSR dataset was generally 300–600 mm higher than that of the CMADS across the whole basin, with the range being 252–1488 mm in the CMADS dataset and 429–2495 mm in the CFSR dataset. There are some studies have found that the precipitation is often overestimated by CFSR datasets [15,20,47]. They indicated that the degree of overestimation of the CFSR data for 2008–2013 was more noticeable than that of other precipitation products; the increase of the precipitation is significant circa 2006. These phenomena may be attributed to single-point observation errors [20,47]. However, there is an exception, in that, the CFSR dataset has an area of less than 300 mm annual precipitation in the upper part of the basin. Lauri et al. [10] also presented data showing a lower average annual precipitation in the upper LMRB over the 1999–2005 period. Lorenz and Kunstmann [13] also concluded that there seems to be a significant bias in the estimation of precipitation at mid to high latitudes by CFSR, which can be explained by the excessive activity in the daily cycle of atmospheric composition over North America [48]. Additionally, some studies found that the CMADS often underestimates precipitation because the daily precipitation recorded by CMORPH satellites always underestimates light rainfall events (due to the interference of surface reflectivity) [15,16,49]. Furthermore, complex orographic features, as well as the effects of the Pacific and Indian Ocean monsoons, are the reasons for the high spatial heterogeneity of the precipitation, which reduces the accuracy of the precipitation both in CMADS and CFSR [15].

The spatial distributions of the annual mean max/min temperatures in the CFSR and CMADS datasets were highly similar; the temperature increased gradually from the upper to lower reaches of the basin. However, both the average annual max/min temperatures of the CFSR were generally lower than those of the CMADS; notably, the maximum temperature of the CFSR is lower in the upper part of the basin, with a negative 6 °C bias. The minimum temperature of the CFSR is generally lower in the whole basin and there were no significant regional differences. Lauri et al. [10] also found that the average annual temperature is lower in the upper LMRB over the 1999–2005 period. Liu et al. [15] found that the maximum and minimum temperatures of CMADS and CFSR were both underestimated in the Qinghai-Tibet Plateau. Wang et al. [47] found that the CFSR temperature anomaly in tropical regions is greater than that in mid to high latitudes.

Notably, the spatial distribution of the annual relative humidity was consistent with that of the annual precipitation, with less relative humidity in the northwest and more relative humidity in the southeast. The relative humidity of the CFSR was generally higher than that of the CMADS in the whole basin. Precipitation is the key factor that affects relative humidity, which may be the main reason that the CFSR has a higher relative humidity than the CMADS. Some studies found that the relative humidity in the CFSR dataset was inaccurate [15,50], as it was higher than in the observations [50]. The spatial distributions of the annual wind speed in the CFSR and CMADS datasets were highly similar, but the wind speed of the CFSR was significantly higher than that of the CMADS in the upper

Preprints (www.preprints.org) | NOT PEER-REVIEWED | Posted: 26 April 2023 doi:10.20944/preprints202304.0983.v1

part of the basin, by approximately 2 m/s. We noted that the wind speed was high in the plateau area, and it decreased gradually with decreasing elevation. It has been demonstrated that wind speed in CFSR and CMADS is overestimated compared with the observed speed in high altitude regions [15,51]. Another significant difference between the CFSR and CMADS was solar radiation. The annual solar radiation of the CFSR was significantly lower than that of the CMADS; in particular, the solar radiation was 1500-MJ/m^2 lower in the downstream region.

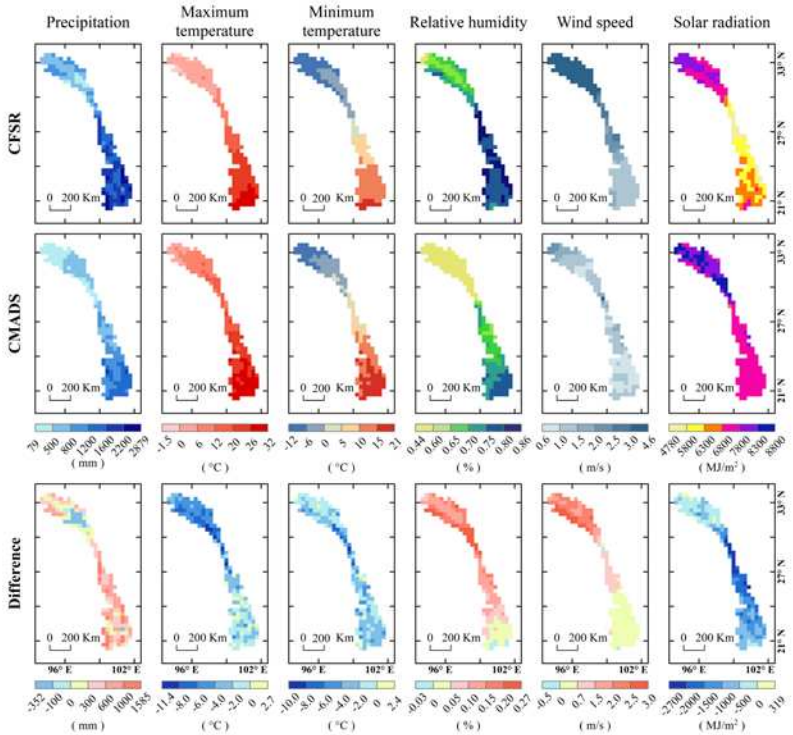

Figure 2. Spatial distribution of the six meteorological variables of the CFSR and CMADS.

3.2. Evaluating the Meteorological Variables of CFSR in the Upper LMRB

After comparing the spatial annual average distribution of the CFSR dataset in the upper LMRB, we evaluated the applicability of the meteorological variables of the CFSR when CMADS was considered as the observational reference. The evaluation indices include R, PBIAS, and RMSE, and the calculation was based on the daily meteorological variables for January 1, 2008 to December 31, 2013. The spatial distributions of the R, PBIAS, and RMSE of the six meteorological variables of CFSR and CMADS are shown in Figure 3. In terms of precipitation, the R values increased from the upstream region to the downstream region, from 0.14 to 0.56, indicating that the precipitation values in the CFSR dataset were accurate in the downstream region. The values of PBIAS were positive almost everywhere in the whole basin, which implies that the precipitation amount in the CFSR was higher than that in the CMADS. The highest positive PBIAS values (above 500) were in the upper part of the basin. However, the negative PBIAS values were also in the upper part of the basin, implying that the precipitation amount in the CFSR were lower than that in the CMADS. Future research is needed to discover why there is this contradiction. The RMSE values increased from the upstream region (2.6) to the downstream region (16.7), indicating that larger deviation of precipitation in the downstream region and smaller deviation in the upstream region.

Preprints (www.preprints.org) | NOT PEER-REVIEWED | Posted: 26 April 2023 doi:10.20944/preprints202304.0983.v1

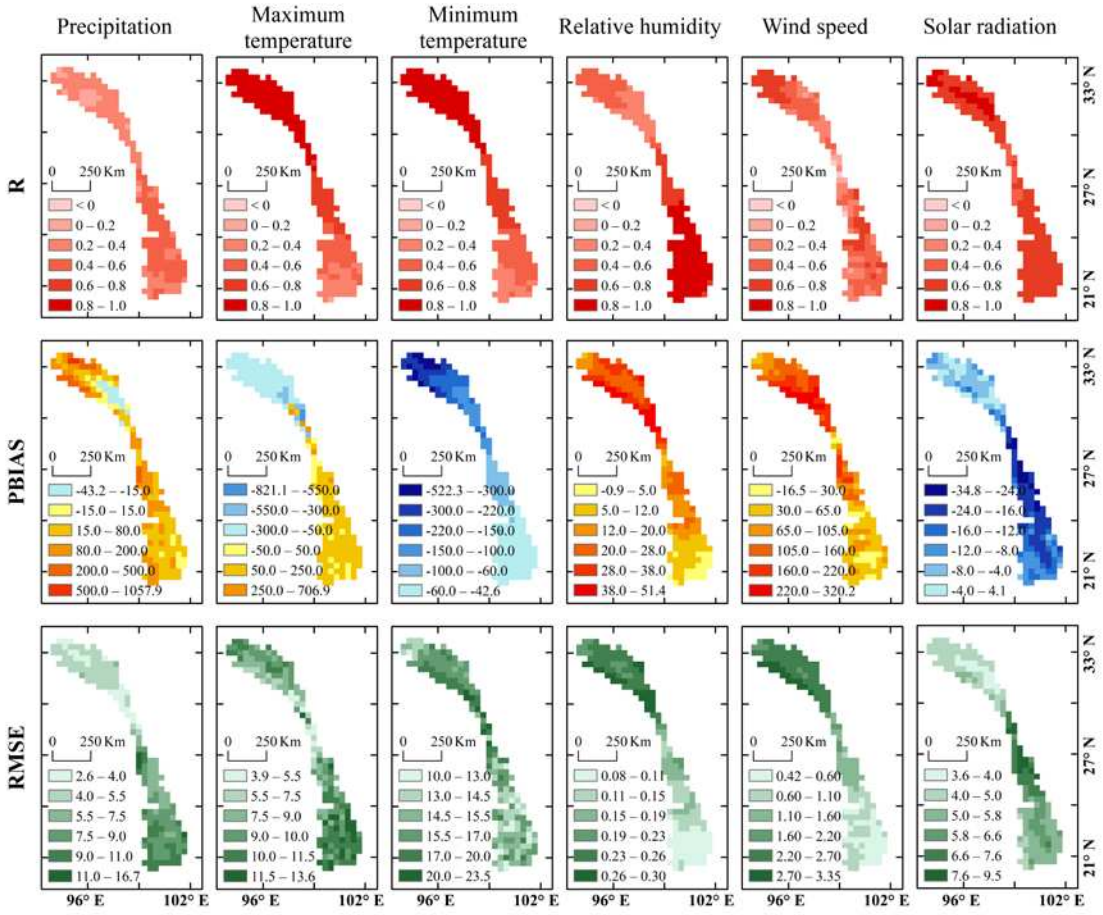

Figure 3. Spatial distributions of R, PBIAS, and RMSE of the six meteorological variables of CFSR and CMADS.

In terms of the max/min temperatures, the R values were positive and high over the entire LMRB, reaching a maximum of 0.95. This indicates that the maximum and minimum temperatures of the CFSR were accurate for most areas. However, there were deviations in the PBIAS and RMSE values. The PBIAS values for maximum temperature were negative in the upstream region, but positive in the downstream region, indicating that the maximum temperatures of the CFSR were lower than that of CMADS in the upstream region, but higher than that of CMADS in the downstream region. Notably, the greatest positive (706.9 %) and negative (–821.1 %) PBIAS values for maximum temperature were observed in the middle and upper reaches of the upper LMRB, implying the great deviation for maximum temperature values between CFSR and CMADS. The PBIAS values for minimum temperature were negative across the whole basin, indicating that the minimum temperatures of the CFSR were lower than that of CMADS. The most negative PBIAS values were observed in the upstream region, and decreased gradually from the upstream to the downstream regions. The RMSE values for maximum and minimum temperatures were similar to the PBIAS results, but the RMSE of the maximum temperature was generally smaller than that of the minimum temperature (10.0 compared to 23.5).

The R values of the relative humidity in the two datasets portrayed a stronger positive correlation in the downstream regions, and the PBIAS and RMSE values of the relative humidity were small in the downstream regions, indicating that the two datasets are highly similar in the downstream regions. However, the deviations of the relative humidity were rather large in the upstream regions, with CFSR values being higher than CMADS values. The R values of the wind speed were moderate, while the PBIAS and RMSE values are small in the upstream regions, indicating that the wind speed of the CFSR was closer to that of the CMADS in the downstream regions. However, deviations in wind speed were positive and large in the upstream regions, where

 doi:10.20944/preprints202304.0983.v1

the wind speed of the CFSR was higher than that of the CMADS. The R of the solar radiation between the CFSR and CMADS was high over the entire basin, and the PBIAS and RMSE values were small in the upstream regions, indicating that the solar radiation of the CFSR was closer to that of the CMADS in the upstream regions. However, the deviations in solar radiation were negative and large in the downstream regions, where the solar radiation of the CFSR was lower than that of the CMADS.

The area average values of the statistical indicators for the six CFSR meteorological variables are shown in Table 1. Note that the indicators for maximum temperature, relative humidity, and solar radiation of the CFSR were close to those of the CMADS with strong correlations (R≥0.65) and small negative deviations (PBIAS≤25%), but the precipitation and wind speed of the CFSR portrayed low correlations (R≤0.50) and large positive deviations (PBIAS≥25%) with those of the CMADS. The minimum temperatures of the CFSR have a high correlation (R is 0.65) and large negative deviations (PBIAS is –127.71%) with that of CMADS. For RMSE, the temperature data portrayed the highest values, in the range of 9–16. The precipitation and solar radiation portrayed moderate values, and the relative humidity and wind speed parameters exhibited the smallest errors.

Table 1. Area average values of the statistical indicators for the six meteorological variables between CFSR and CMADS.

Meteorological Variables	R	PBIAS	RMSE
Precipitation	0.35	85.47	6.68
Maximum temperature	0.68	-18.45	9.39
Minimum temperature	0.65	-127.71	15.71
Relative humidity	0.65	20.01	0.18
Wind speed	0.47	103.36	1.52
Solar radiation	0.72	-12.11	5.45

3.3. Comparison of the Hydrological Features between CFSR-Based SWAT+ and CMADS-Based SWAT+

3.3.1. Model Parameter Sensitivity Based on the CFSR and CMADS

In order to compare the hydrological features based on two different meteorological re-analyses in the upper LMRB, we first needed to compare the model parameter sensitivity. We used Sobol's method to screen the sensitive parameters. Figure 4 portrays the first order sensitivities of a total of 24 commonly used parameters based on the two different meteorological re-analyses, the CFSR and CMADS. We noted that the sensitive parameters based on the CFSR, where the first order sensitivity was greater than 0, were highly consistent with those based on the CMADS. However, the sensitivity of these parameters (in terms of both the datasets) were different. Overall, we determined 17 consistent sensitive parameters: esco, k, snomelt_tmp, awc, lat_ttime, snofall_tmp, perco, slope, alpha, snomelt_lag, snomelt_min, revap_co, surlag, canmx, epco, cn2, and snomelt_max. Two sensitive parameters were inconsistent: flo_min, which was sensitive based on the CFSR only, and revap_min, which was sensitive based on the CMADS only. Finally, we chose all 19 sensitive parameters, both consistent and inconsistent, for which the first order sensitivity was greater than 0 in both the CFSR and CMADS, to carry out parameter calibration and validation.

Preprints (www.preprints.org) | NOT PEER-REVIEWED | Posted: 26 April 2023 doi:10.20944/preprints202304.0983.v1

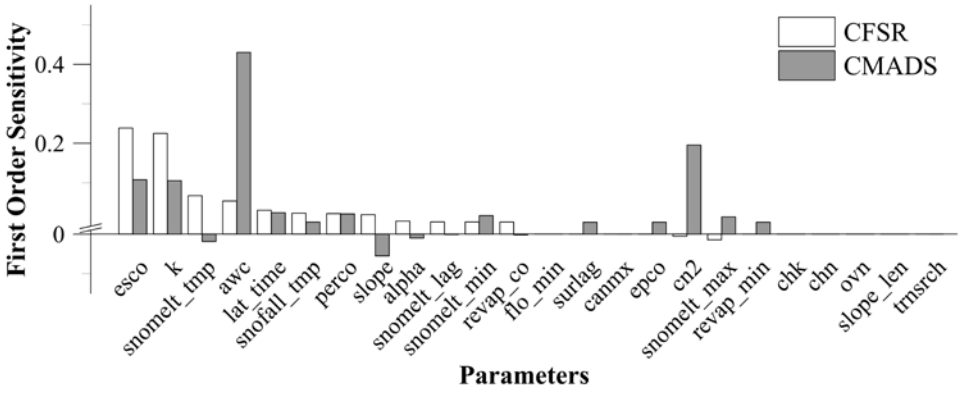

Figure 4. First order sensitivity of 24 commonly used parameters for streamflow simulation based on the two different meteorological re-analyses, CFSR and CMADS, under Sobol's method.

Note: soil evaporation compensation factor (esco), saturated hydraulic conductivity of soil layer (k), snowmelt temperature (snomelt_tmp), available water capacity of soil layer (awc), lateral flow travel time (lat_ttime), snowfall temperature (snofall_tmp), percolation coefficient (perco), average slope steepness in HRU (slope), alpha factor for groundwater recession curve (alpha), snowmelt lag factor (snomelt_lag), minimum snowmelt temperature (snomelt_min), fraction of pet to calculate revap (revap_co), minimum aquifer storage to allow return flow (flo_min), surface-runoff lag time (surlag), maximum canopy storage (canmx), plant water-uptake compensation factor (epco), soil conservation service (SCS) runoff curve number adjustment factor (cn2), and maximum snowmelt temperature (snomelt_max), threshold depth of water in shallow aquifer required to allow revap to occur (revap_min), effective hydraulic conductivity of main channel alluvium (chk), Manning's "n" value for the main channel (chn), Manning's "n" value for overland flow (ovn), average slope length for erosion (slope_len), and fraction of transmission losses from main channel that enter deep aquifer (trmsrch)

3.3.2. Model Calibration and Validation Based on CFSR and CMADS

To further assess the capability of the SWAT+ hydrological model for streamflow simulations based on the two different meteorological re-analyses in the upper LMRB, we used DDS for the model parameters calibration, and then used streamflow simulation for validation using the observed monthly streamflow at Chiang Sean hydrological station. The hydrological simulation period was from January 2008 to December 2013. We chose 2008, one year, as the warm-up period, 3 years from 2009 to 2011 as the calibration period, and 2 years from 2012 to 2013 as the validation period. Table 2 portrays the calibrated optimal values, and the value range and change types of the 19 sensitive parameters for each meteorological reanalysis. The calibrated optimal values of the 19 sensitive parameters were very different for the two meteorological re-analyses, with these differences being reflected mainly in the most sensitive parameters, including esco, slope, epco, and surlag. Of note, the optimal values of the parameters were positive for the CFSR but negative for the CMADS. This was seen in, for example, awc. Note that esco, revap_min and awc all affect the process of evaporation. To adjust for the higher precipitation of CFSR, the evaporation based on CFSR may need a greater value. However, the calibrated optimal values of some parameters were consistent, including revap_co, cn2, lat_ttime, and perco. Based on the results comparison of the re-analyses as explained in Sections 4.1 and 4.2, the differences in the meteorological re-analyses may be the reason for the different calibrated optimal values.

Preprints (www.preprints.org) | NOT PEER-REVIEWED | Posted: 26 April 2023 doi:10.20944/preprints202304.0983.v1

Table 2. The calibrated optimal values of the 19 sensitive parameters for SWAT+ based on the two meteorological re-analyses, namely, CFSR and CMADS.

Parameters	Min	Max	Change Type*	Parameter Group	Optimal Values	
					CFSR	CMADS
esco	0	1	replace	HRU	0.274	0.072
slope	-50	50	relative	HRU	2.377	47.689
revap_co	0.02	0.2	replace	Aquifer	0.184	0.198
epco	0	1	replace	HRU	0.046	0.717
canmx	0	100	replace	HRU	46.584	30.641
surlag	0.05	24	replace	Basin	2.738	13.966
alpha	0	1	replace	Aquifer	0.075	0.264
awc	-25	25	relative	Soil	15.516	-15.443
cn2	-20	20	relative	HRU	-19.682	-18.928
flo_min	0	5000	replace	Aquifer	1704.311	3329.009
k	-80	80	relative	Soil	78.688	42.922
lat_ttime	0.5	180	replace	HRU	118.878	126.252
revap_min	0	500	replace	Aquifer	451.913	231.766
snofall_tmp	-5	5	replace	HRU	3.482	4.602
snomelt_lag	0	1	replace	HRU	0.591	0.976
snomelt_max	0	10	replace	HRU	3.314	0.235
snomelt_min	0	10	replace	HRU	8.177	4.773
snomelt_tmp	-5	5	replace	HRU	-2.919	-3.637
perco	0	1	replace	HRU	0.901	0.773

Note: *Relative change: increases/ decreases the current value by a specified value; Replace: the specified value takes the place of the old parameter value.

Two simulated monthly streamflows, based on the corresponding calibrated SWAT+ model parameters forced by the two different meteorological re-analyses, with the observed monthly streamflow at the Chiang Sean hydrological station during the calibration period (2009–2010) and validation period (2011–2013) periods, are shown in Figure 5. The statistical measures used to evaluate the simulated streamflow included the NSE coefficient, PBIAS, and R^2. The higher the values of NSE and R^2, the smaller the value of PBIAS and the more accurate the simulated streamflow. Both the simulated monthly streamflow performed well during the calibration period, with NSE values all greater than 0.8, R^2 values greater than 0.88, and PBIAS values less than 15 %. The performances were still good during the validation period, with NSE values greater than 0.65, R^2 values greater than 0.70, and PBIAS values less than 11 %. Overall, the model performance driven by the CFSR dataset was better than that driven by the CMADS dataset, with higher NSE and R^2 values and the smaller PBIAS values. According to the hydrograph in Figure 5, the CFSR-based and CMADS-based SWAT+ simulated streamflow can essentially simulate the observed peak and low streamflow, but the CMADS-based SWAT+ simulated streamflow tended to underestimate the peak and low streamflow. Therefore, we noted that CFSR met the demands for simulating streamflow through SWAT+ hydrological model in the upper LMRB.

Preprints (www.preprints.org) | NOT PEER-REVIEWED | Posted: 26 April 2023 doi:10.20944/preprints202304.0983.v1

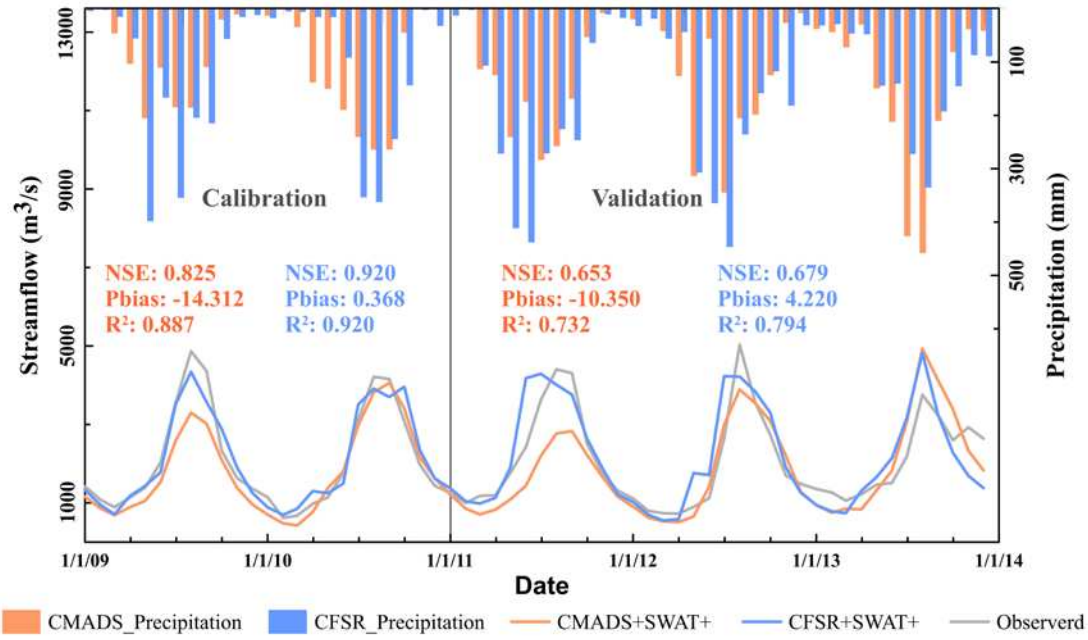

Figure 5. Comparison of the simulated monthly streamflow, based on the corresponding calibrated SWAT+ model parameters forced by the two different meteorological reanalyses, with the observed monthly streamflow and precipitation at the Chiang Sean hydrological station during the calibration (2009–2010) and validation (2011–2013) periods.

To understand the mechanism behind the simulated monthly streamflow, we analyzed the simulated water balance based on the corresponding calibrated SWAT+ model parameters forced by the two different meteorological re-analyses, as shown in Figure 6, which were obtained from the model check component in the SWAT+ Editor. Although the precipitation in the CFSR-based SWAT+ simulation was much higher than that in the CMADS-based SWAT+ simulation across the entire basin, only 49% of the precipitation of CFSR is converted to streamflow while 82% of the precipitation of CMADS is converted. Furthermore, the evaporation and transpiration (ET) in the CFSR-based SWAT+ simulation were also higher than that in the CMADS-based SWAT+ simulation, which may be another reason that the CFSR-based and CMADS-based SWAT+ simulated streamflow did not differ greatly. The higher percolation and baseflow in the CMADS-based SWAT+ simulation may lead to the lower simulated peak and low streamflow. Several factors can cause different responses between the meteorological estimates and hydrological outputs, including the sensitive parameters and their calibrated optimal values in the SWAT+ hydrological model. Gao et al. [14] concluded that the conversion of precipitation to runoff is a highly complex nonlinear process. Therefore, the discrepancies between the two meteorological forcings do not transfer linearly to runoff. This may result in significant differences in the simulated streamflow forced by the two different meteorological re-analyses, CFSR and CMADS.

Preprints (www.preprints.org) | NOT PEER-REVIEWED | Posted: 26 April 2023 doi:10.20944/preprints202304.0983.v1

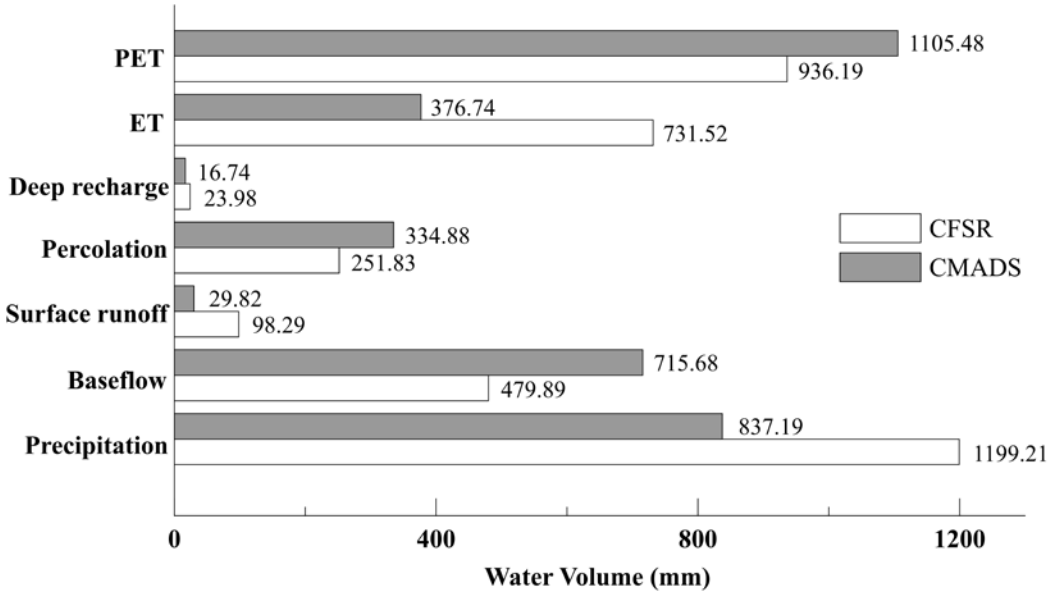

Figure 6. Simulated water balance based on the corresponding calibrated SWAT+ model parameters forced by the two different meteorological re-analyses, CFSR and CMADS.

4. Discussion

4.1. Differences in Meteorological Forcings

Several previous studies have compared the meteorological elements of global or local re-analyses with gauge-observed data [10,13,14,16,20]. Such comparisons may introduce errors and uncertainties between the re-analyses and the gauged observations due to spatial scale differences. However, a comparison between re-analyses and grided observed data, such as the CMADS, can improve our understanding of how meteorological elements behave [52]. For the comparison of the precipitation and temperature between global atmospheric re-analyses and the observed data, Tian et al. [52] concluded that precipitation of the CFSR is higher than the observed data and CMADS, while the maximum/minimum temperatures of the CFSR are generally lower than the observed data and CMADS. These findings are also consistent with the results of another study on the Mekong River basin [10].

The comprehensive meteorological datasets of the CMADS render the comparison of the other meteorological variables (wind speed, relative humidity, and solar radiation) of the CFSR in the upper LMRB possible. Our results found that the precipitation, relative humidity, and wind speed of the CFSR were higher than those of the CMADS, while the max/min temperatures and solar radiation were lower than those of the CMADS. There is a need to investigate the reason why the temperatures and solar radiation of the CFSR are lower than those of the CMADS and why the CFSR exhibits higher wind speeds than does the CMADS. Meng et al. [26] concluded that temperature has a relatively greater RMSE in the southern and western parts of the Yunnan province, and a minority of stations in the region show negative biases when compared to the observations from the national automatic stations. Relative humidity and wind speed showed positive bias effect in the southern parts of the Yunnan province [26]. However, the factors influencing the accuracy of CMADS have not yet been systematically analyzed [26]. The main reason for the differences between the CMADS and CFSR was the differences in the observation data source and assimilation methods. The observation data source of the CMADS included about 40,000 regional encrypted stations that observed various surface meteorological elements, 2421 automatic stations, and 131 radar detection stations [26]. The LAPS/STMAS system, a comprehensive analytical system, was adopted to assimilate the source data in the CMADS. The CFSR data were acquired using a multi-source data assimilation system. For example, the precipitation of CMADS is mainly based on the global precipitation products from

CMORPH adjusted by observed precipitation [26]. However, the precipitation of CFSR is generated by merging the CFSR background precipitation, global daily gauge analysis and the satellite precipitation [25]. We note that it is normal for the meteorological data of the CFSR and CMADS to be different, despite quality control being carried out for both datasets.

4.2. Differences in Hydrological Model Response

Various studies have reported that the performance of meteorological re-analyses in discharge modeling varies depending on the situation compared to rain gauge data [10,11,14–17,20]. However, their results indicate that the CFSR could be a valuable option for hydrological simulation in areas with limited data. In this study, we compared the hydrological responses between the CFSR-based SWAT+ simulation and the CMADS-based SWAT+ simulation under the same watershed delineation, hydrological model, parameter sensitivity analysis, and calibration method. However, two different meteorological re-analyses led to different sensitivity and calibrated optimal values of the consistent parameters, which further led to a different hydrological response. Moreover, the simulations with the CFSR and CMADS yielded significant differences in the water balance components in the upper LMRB. For example, higher precipitation led to a lower conversion rate to streamflow and higher evaporation and transpiration, according to the water balance in this study. Therefore, a different watershed delineation, hydrological model, the parameter sensitivity analysis, and calibration method would lead to different hydrological responses. In order to make hydrological simulation more efficient in evaluating the performance of meteorological re-analyses in discharge modeling, we created four subbasins and 110 HRUs from the DEM by specifying the default area thresholds for channel (1716 km^2) and for stream (17160 km^2). As the small area thresholds create more subbasins and HRUs, they require more computing time for hydrological simulation, which may affect the hydrological responses.

The comprehensive meteorological datasets for hydrological modeling are beneficial in understanding the hydrological responses and water balance components. The availability of wind speed, relative humidity, and solar radiation data in the CFSR and the CMADS makes calculating hydrological components in watersheds more flexible. For example, this study used the Penman–Montieth methods to calculate PET, while other studies were limited by the use of the Hargreaves method to calculate PET [17], which only requires maximum and minimum temperatures.

4.3. Limitations

In addition to the input meteorological data and hydrological model parameters, anthropogenic activities can influence streamflow simulation, especially due to reservoir and dam construction. Lu et al. [53] concluded that Chinese dams can reduce the low water-discharge and monthly mean values of water discharge averaged through the entire pre- and post-dam period, with the largest decrease occurring in Summer. Han et al. [2] concluded that the mean annual streamflow changed significantly after construction of the large hydropower plant, Nuozhadu, began, inferring that anthropogenic activities contributed to ~ 43–95 % of this change. Reservoir construction was the most significant factor affecting the streamflow in the region; other anthropogenic activities that affected the streamflow were agricultural, industrial, and domestic water use [2]. In this present study, we focused on how the CFSR meteorological datasets influenced the streamflow driven by the SWAT+ model simulation of the upper LMRB. Future studies should focus on the impact of anthropogenic activities, such as reservoir and dam construction and agricultural irrigation, on the streamflow simulation in the upper LMRB.

5. Conclusions

Our study aimed to assess the different hydrological responses through hydrological modeling in the upper LMRB using the two common open gridded meteorological datasets, CFSR and CMADS. This study evaluated the suitability of six meteorological variables from the CFSR and CMADS that

are commonly used to force the SWAT+ model, along with analyzing the differences in the hydrological modeling. We arrived at the following conclusions:

All the meteorological variables of the CFSR and CMADS datasets exhibited similar spatial average annual distributions; however, precipitation, relative humidity, and wind speed in the CFSR were greater than those in the CMADS. Further, the temperatures and solar radiation were lower in the CFSR. The spatial distributions of the statistical indicators in the CFSR and CMADS, namely, the R, PBIAS, and RMSE values, were different. The temperatures and solar radiation in the CFSR and CMADS exhibited strong correlations across the entire basin, while precipitation and relative humidity portrayed strong correlations in the downstream regions. Additionally, wind speed exhibited an irregular spatial distribution of correlation over the entire river basin. The PBIAS results indicated that precipitation, relative humidity, and wind speed portrayed positive deviations across the entire basin. Minimum temperature and solar radiation portrayed negative deviations across the entire basin. Notably, the maximum temperature yielded a positive deviation in the downstream and a negative deviation in the upstream regions. These conclusions were further confirmed by the result of RMSE and the area average values of the statistical indicators.

For a comparison of the hydrological features of the CFSR- and CMADS-based SWAT+ models, we compared the sensitive parameters and simulated the monthly streamflow. Different meteorological datasets resulted in significant differences of hydrological responses, which reflected by different sensitive parameters and their optimal value. Nineteen sensitive parameters (from the total of 24 parameters) for the CFSR and CMADS models were mostly the same, with only 2 being inconsistent, namely flo_min and revap_min. However, the sensitivities of these parameters were different. The calibrated optimal values of the 19 sensitive parameters were very different for the two meteorological re-analyses, reflected mainly in the most sensitive parameters, including esco, slope, epco, and surlag. These different calibrated optimal values of sensitive parameters further lead to the different simulated water balance components between CFSR- and CMADS-based SWAT+ model. The monthly streamflow simulated using the CFSR-based SWAT+ model was superior to that simulated using the CMADS-based SWAT+ model from 2008-2013, with higher NSE and lower PBIAS values. These results indicate that CFSR can better meet the demand of driving the SWAT+ model to simulate the streamflow in the upper LMRB. This study advances our understanding of the strengths and weaknesses of different meteorological forcings and their performances, and helps to determine the applicable hydrological models for the upper LMRB.

Supplementary Materials: Figure S1: Map of land use/land cover distribution in the upper Lancang-Mekong River Basin; Table S1: Dominant Land Cover Classes in the upper Lancang-Mekong River Basin; Figure S2: Map of soil type distribution in the upper Lancang-Mekong River Basin; Table S2: Major Soil Types in the upper Lancang-Mekong River Basin; Figure S3: The channels and streams in the upper Lancang-Mekong River basin.

Author Contributions: Investigation, S.Z., F.Y. and Y.G.; Methodology, Y.L.; Software, S.Z., Y.L., X.Q. and X.L.; Supervision, Y.L., L.L. and Q.D.; Writing – original draft, S.Z., Y.L. and F.Y.; Writing – review & editing, Y.L., Qi Yi, L.L. and Q.D. All authors have read and agreed to the published version of the manuscript.

Funding: This research was funded by the National Natural Science Foundation of China (Grant numbers 41907147, 41761109); Research and Innovation Fund for Graduate Students of the Yunnan University (Grant numbers 2021Y350); and Innovation and Entrepreneurship Training Fund for Undergraduate Students of the Yunnan University (Grant numbers 202110673101).

Data Availability Statement: The CFSR and CMADS used in this study are publicly available meteorological reanalyses and can be downloaded from their official websites respectively (https://swat.tamu.edu/data/cfsr; http://www.cmads.org/); SRTM Non-Void Filled (Digital Object Identifier (DOI) number: /10.5066/F7K072R7) can be downloaded from https://earthexplorer.usgs.gov/, and the landuse and soil data can be downloaded from https://swat.tamu.edu/data/.

Acknowledgments: We would like to thank Texas A&M University for providing the free SWAT+ version 2.0.6 based on QSWAT+ platform and SWAT+ Toolbox v1.0 model and the two meteorological re-analyses, CFSR and CMADS, required to conduct this study.

Conflicts of Interest: The authors declare no conflict of interest.

Abbreviations:

NCEP	National Centers for Environmental Prediction
HRU	Hydrological response unit
DEMs	Digital elevation models
LULC	Land use/land cover
LAPS/STMAS	Local Analysis and Prediction System/Space-Time Multiscale Analysis System
CPC	Climate Prediction Center
CMORPH	Climate Prediction Center morphing
USGS	United States Geological Survey
ET	Evaporation and transpiration
PET	Potential evapotranspiration

References

1. IPCC. Climate Change 2022: Impacts, Adaptation, and Vulnerability. Contribution of Working Group II to the Sixth Assessment Report of the Intergovernmental Panel on Climate Change. **2022,** CAMBRIDGE UNIV PRESS UK: CAMBRIDGE, doi:10.1017/9781009325844.
2. Han, Z.; Long, D.; Fang, Y.; Hou, A.; Hong, Y. Impacts of Climate Change and Human Activities on the Flow Regime of the Dammed Lancang River in Southwest China. *Journal of Hydrology* **2019**, *570*, 96–105. https://doi.org/10.1016/j.jhydrol.2018.12.048
3. Liu, J.; Chen, D.; Mao, G.; Irannezhad, M.; Pokhrel, Y. Past and Future Changes in Climate and Water Resources in the Lancang–Mekong River Basin: Current Understanding and Future Research Directions. *Engineering* **2022**, *13*, 144–152. https://doi.org/10.1016/j.eng.2021.06.026
4. Räsänen, T. A.; Kummu, M. Spatiotemporal Influences of ENSO on Precipitation and Flood Pulse in the Mekong River Basin. *Journal of Hydrology* **2013**, *476*, 154–168. https://doi.org/10.1016/j.jhydrol.2012.10.028
5. Pokhrel, Y.; Burbano, M.; Roush, J.; Kang, H.; Sridhar, V.; Hyndman, D. A Review of the Integrated Effects of Changing Climate, Land Use, and Dams on Mekong River Hydrology. *Water* **2018**, *10* (3), 266. https://doi.org/10.3390/w10030266
6. Hoang, L. P.; van Vliet, M. T. H.; Kummu, M.; Lauri, H.; Koponen, J.; Supit, I.; Leemans, R.; Kabat, P.; Ludwig, F. The Mekong's Future Flows under Multiple Drivers: How Climate Change, Hydropower Developments and Irrigation Expansions Drive Hydrological Changes. *Science of The Total Environment* **2019**, *649*, 601–609. https://doi.org/10.1016/j.scitotenv.2018.08.160
7. Try, S.; Tanaka, S.; Tanaka, K.; Sayama, T.; Khujanazarov, T.; Oeurng, C. Comparison of CMIP5 and CMIP6 GCM Performance for Flood Projections in the Mekong River Basin. *Journal of Hydrology: Regional Studies* **2022**, *40*, 101035. https://doi.org/10.1016/j.ejrh.2022.101035
8. Hirabayashi, Y.; Mahendran, R.; Koirala, S.; Konoshima, L.; Yamazaki, D.; Watanabe, S.; Kim, H.; Kanae, S. Global Flood Risk under Climate Change. *Nature Clim Change* **2013**, *3* (9), 816–821. https://doi.org/10.1038/nclimate1911
9. Wang, W.; Lu, H.; Ruby Leung, L.; Li, H.-Y.; Zhao, J.; Tian, F.; Yang, K.; Sothea, K. Dam Construction in Lancang-Mekong River Basin Could Mitigate Future Flood Risk From Warming-Induced Intensified Rainfall: Dam Mitigate Flood Risk in Mekong. *Geophys. Res. Lett.* **2017**, *44* (20), 10,378-10,386. https://doi.org/10.1002/2017GL075037
10. Lauri, H.; Räsänen, T. A.; Kummu, M. Using Reanalysis and Remotely Sensed Temperature and Precipitation Data for Hydrological Modeling in Monsoon Climate: Mekong River Case Study. *Journal of Hydrometeorology* **2014**, *15* (4), 1532–1545. https://doi.org/10.1175/JHM-D-13-084.1
11. Fuka, D. R.; Walter, M. T.; MacAlister, C.; Degaetano, A. T.; Steenhuis, T. S.; Easton, Z. M. Using the Climate Forecast System Reanalysis as Weather Input Data for Watershed Models: USING CFSR AS WEATHER INPUT DATA FOR WATERSHED MODELS. *Hydrol. Process.* **2014**, *28* (22), 5613–5623. https://doi.org/10.1002/hyp.10073
12. Tan, M. L.; Gassman, P. W.; Liang, J.; Haywood, J. M. A Review of Alternative Climate Products for SWAT Modelling: Sources, Assessment and Future Directions. *Science of The Total Environment* **2021**, *795*, 148915. https://doi.org/10.1016/j.scitotenv.2021.148915
13. Lorenz, C.; Kunstmann, H. The Hydrological Cycle in Three State-of-the-Art Reanalyses: Intercomparison and Performance Analysis. *JOURNAL OF HYDROMETEOROLOGY* **2012**, *13*, 24
14. Gao, X.; Zhu, Q.; Yang, Z.; Wang, H. Evaluation and Hydrological Application of CMADS against TRMM 3B42V7, PERSIANN-CDR, NCEP-CFSR, and Gauge-Based Datasets in Xiang River Basin of China. *Water* **2018**, *10* (9), 1225. https://doi.org/10.3390/w10091225
15. Liu, J.; Shanguan, D.; Liu, S.; Ding, Y. Evaluation and Hydrological Simulation of CMADS and CFSR Reanalysis Datasets in the Qinghai-Tibet Plateau. *Water* **2018**, *10* (4), 513. https://doi.org/10.3390/w10040513

16. Zhang, L.; Meng, X.; Wang, H.; Yang, M.; Cai, S. Investigate the Applicability of CMADS and CFSR Reanalysis in Northeast China. *Water* **2020**, *12* (4), 996. https://doi.org/10.3390/w12040996
17. Dile, Y. T.; Srinivasan, R. Evaluation of CFSR Climate Data for Hydrologic Prediction in Data-Scarce Watersheds: An Application in the Blue Nile River Basin. *J Am Water Resour Assoc* **2014**, *50* (5), 1226–1241. https://doi.org/10.1111/jawr.12182
18. Meng, X.; Wang, H. Significance of the China Meteorological Assimilation Driving Datasets for the SWAT Model (CMADS) of East Asia. *Water* **2017**, *9* (10), 765. https://doi.org/10.3390/w9100765
19. Meng; Wang; Chen. Profound Impacts of the China Meteorological Assimilation Dataset for SWAT Model (CMADS). *Water* **2019**, *11* (4), 832. https://doi.org/10.3390/w11040832
20. Wang, N.; Liu, W.; Sun, F.; Yao, Z.; Wang, H.; Liu, W. Evaluating Satellite-Based and Reanalysis Precipitation Datasets with Gauge-Observed Data and Hydrological Modeling in the Xihe River Basin, China. *Atmospheric Research* **2020**, *234*, 104746. https://doi.org/10.1016/j.atmosres.2019.104746
21. Salathé, E. P. Comparison of Various Precipitation Downscaling Methods for the Simulation of Streamflow in a Rainshadow River Basin: PRECIPITATION DOWNSCALING METHODS FOR STREAMFLOW SIMULATION. *Int. J. Climatol.* **2003**, *23* (8), 887–901. https://doi.org/10.1002/joc.922
22. Zhang, B. A Water-Energy Balance Approach for Multi-Category Drought Assessment across Globally Diverse Hydrological Basins. *Agricultural and Forest Meteorology* **2019**, 19
23. Vrugt, J. A.; Bouten, W.; Gupta, H. V.; Sorooshian, S. Toward Improved Identifiability of Hydrologic Model Parameters: The Information Content of Experimental Data: IMPROVED IDENTIFIABILITY OF HYDROLOGIC MODEL PARAMETERS. *Water Resour. Res.* **2002**, *38* (12), 48-1-48–13. https://doi.org/10.1029/2001WR001118
24. Yapo, P. O.; Gupta, H. V.; Sorooshian, S. Multi-Objective Global Optimization for Hydrologic Models. *Journal of Hydrology* **1998**, *204* (1–4), 83–97. https://doi.org/10.1016/S0022-1694(97)00107-8
25. Saha, S.; Moorthi, S.; Pan, H.-L.; Wu, X.; Wang, J.; Nadiga, S.; Tripp, P.; Kistler, R.; Woollen, J.; Behringer, D.; Liu, H.; Stokes, D.; Grumbine, R.; Gayno, G.; Wang, J.; Hou, Y.-T.; Chuang, H.; Juang, H.-M. H.; Sela, J.; Iredell, M.; Treadon, R.; Kleist, D.; Van Delst, P.; Keyser, D.; Derber, J.; Ek, M.; Meng, J.; Wei, H.; Yang, R.; Lord, S.; van den Dool, H.; Kumar, A.; Wang, W.; Long, C.; Chelliah, M.; Xue, Y.; Huang, B.; Schemm, J.-K.; Ebisuzaki, W.; Lin, R.; Xie, P.; Chen, M.; Zhou, S.; Higgins, W.; Zou, C.-Z.; Liu, Q.; Chen, Y.; Han, Y.; Cucurull, L.; Reynolds, R. W.; Rutledge, G.; Goldberg, M. The NCEP Climate Forecast System Reanalysis. *Bull. Amer. Meteor. Soc.* **2010**, *91* (8), 1015–1058. https://doi.org/10.1175/2010BAMS3001.1
26. Meng, X.; Wang, H.; Shi, C.; Wu, Y.; Ji, X. Establishment and Evaluation of the China Meteorological Assimilation Driving Datasets for the SWAT Model (CMADS). *Water* **2018**, *10* (11), 1555. https://doi.org/10.3390/w10111555
27. FAO. World Soil Resources. An Explanatory Note on the FAO World Soil Resources Map at 1 : 25,000,000 Scale. **1992**
28. Yihun Dile; R Srinivasan; George, C. Manual for QSWAT. QSWAT Is the SWAT Interface for QGIS. SWAT (Soil and Water Assessment Tool) Is a Physically Based Hydrological Model. **2015**. https://doi.org/10.13140/RG.2.1.1060.7201
29. Bieger, K.; Arnold, J. G.; Rathjens, H.; White, M. J.; Bosch, D. D.; Allen, P. M.; Volk, M.; Srinivasan, R. Introduction to SWAT+, A Completely Restructured Version of the Soil and Water Assessment Tool. *J Am Water Resour Assoc* **2017**, *53* (1), 115–130. https://doi.org/10.1111/1752-1688.12482
30. Neitsch, S. L.; Arnold, J. G.; Kiniry, J. R.; Williams, J. R. *Soil and Water Assessment Tool Theoretical Documentation Version 2009*; Technical Report; Texas Water Resources Institute, 2011. https://oaktrust.library.tamu.edu/handle/1969.1/128050 (accessed 2023-04-23)
31. Sorooshian, S.; Duan, Q.; Gupta, V. K. Calibration of Rainfall-Runoff Models: Application of Global Optimization to the Sacramento Soil Moisture Accounting Model. *Water Resour. Res.* **1993**, *29* (4), 1185–1194. https://doi.org/10.1029/92WR02617
32. Yapo, P. O.; Gupta, H. V.; Sorooshian, S. Automatic Calibration of Conceptual Rainfall-Runoff Models: Sensitivity to Calibration Data. *Journal of Hydrology* **1996**, *181* (1–4), 23–48. https://doi.org/10.1016/0022-1694(95)02918-4
33. Nash, J. E.; Sutcliffe, J. V. River Flow Forecasting through Conceptual Models Part I — A Discussion of Principles. *Journal of Hydrology* **1970**, *10* (3), 282–290. https://doi.org/10.1016/0022-1694(70)90255-6
34. D. N. Moriasi; J. G. Arnold; M. W. Van Liew; R. L. Bingner; R. D. Harmel; T. L. Veith. Model Evaluation Guidelines for Systematic Quantification of Accuracy in Watershed Simulations. *Transactions of the ASABE* **2007**, *50* (3), 885–900. https://doi.org/10.13031/2013.23153
35. Li, J.; Duan, Q. Y.; Gong, W.; Ye, A.; Dai, Y.; Miao, C.; Di, Z.; Tong, C.; Sun, Y. Assessing Parameter Importance of the Common Land Model Based on Qualitative and Quantitative Sensitivity Analysis. *Hydrol. Earth Syst. Sci.* **2013**, *17* (8), 3279–3293. https://doi.org/10.5194/hess-17-3279-2013
36. Zhang, C.; Chu, J.; Fu, G. Sobol"s Sensitivity Analysis for a Distributed Hydrological Model of Yichun River Basin, China. *Journal of Hydrology* **2013**, *480*, 58–68. https://doi.org/10.1016/j.jhydrol.2012.12.005

37. Massmann, C.; Holzmann, H. Analysis of the Behavior of a Rainfall–Runoff Model Using Three Global Sensitivity Analysis Methods Evaluated at Different Temporal Scales. *Journal of Hydrology* **2012**, *475*, 97–110. https://doi.org/10.1016/j.jhydrol.2012.09.026
38. Khorashadi Zadeh, F.; Nossent, J.; Sarrazin, F.; Pianosi, F.; van Griensven, A.; Wagener, T.; Bauwens, W. Comparison of Variance-Based and Moment-Independent Global Sensitivity Analysis Approaches by Application to the SWAT Model. *Environmental Modelling & Software* **2017**, *91*, 210–222. https://doi.org/10.1016/j.envsoft.2017.02.001
39. Brouziyne, Y.; Abouabdillah, A.; Bouabid, R.; Benaabidate, L.; Oueslati, O. SWAT Manual Calibration and Parameters Sensitivity Analysis in a Semi-Arid Watershed in North-Western Morocco. *Arab J Geosci* **2017**, *10* (19), 427. https://doi.org/10.1007/s12517-017-3220-9
40. White, K. L.; Chaubey, I. SENSITIVITY ANALYSIS, CALIBRATION, AND VALIDATIONS FOR A MULTISITE AND MULTIVARIABLE SWAT MODEL. *J Am Water Resources Assoc* **2005**, *41* (5), 1077–1089. https://doi.org/10.1111/j.1752-1688.2005.tb03786.x
41. Li, M.; Di, Z.; Duan, Q. Effect of Sensitivity Analysis on Parameter Optimization: Case Study Based on Streamflow Simulations Using the SWAT Model in China. *Journal of Hydrology* **2021**, *603*, 126896. https://doi.org/10.1016/j.jhydrol.2021.126896
42. Sobol, I. M. Sensitivity estimates for nonlinear mathematical models. *Mathematical Modelling and Computational Experiments* **1993**, 1(1), 112–118.
43. Abbaspour, K.; Vaghefi, S.; Srinivasan, R. A Guideline for Successful Calibration and Uncertainty Analysis for Soil and Water Assessment: A Review of Papers from the 2016 International SWAT Conference. *Water* **2017**, *10* (1), 6. https://doi.org/10.3390/w10010006
44. Tolson, B. A.; Shoemaker, C. A. Dynamically Dimensioned Search Algorithm for Computationally Efficient Watershed Model Calibration: DYNAMICALLY DIMENSIONED SEARCH ALGORITHM. *Water Resour. Res.* **2007**, *43* (1). https://doi.org/10.1029/2005WR004723
45. Yen, H.; Wang, X.; Fontane, D. G.; Harmel, R. D.; Arabi, M. A Framework for Propagation of Uncertainty Contributed by Parameterization, Input Data, Model Structure, and Calibration/Validation Data in Watershed Modeling. *Environmental Modelling & Software* **2014**, *54*, 211–221. https://doi.org/10.1016/j.envsoft.2014.01.004
46. Yen, H.; Jeong, J.; Smith, D. R. Evaluation of Dynamically Dimensioned Search Algorithm for Optimizing SWAT by Altering Sampling Distributions and Searching Range. *J Am Water Resour Assoc* **2016**, *52* (2), 443–455. https://doi.org/10.1111/1752-1688.12394
47. Wang, W.; Xie, P.; Yoo, S.-H.; Xue, Y.; Kumar, A.; Wu, X. An Assessment of the Surface Climate in the NCEP Climate Forecast System Reanalysis. *Clim Dyn* **2011**, *37* (7–8), 1601–1620. https://doi.org/10.1007/s00382-010-0935-7
48. Higgins, R. W.; Kousky, V. E.; Silva, V. B. S.; Becker, E.; Xie, P. Intercomparison of Daily Precipitation Statistics over the United States in Observations and in NCEP Reanalysis Products. *Journal of Climate* **2010**, *23* (17), 4637–4650. https://doi.org/10.1175/2010JCLI3638.1
49. Beck, H. E.; van Dijk, A. I. J. M.; Levizzani, V.; Schellekens, J.; Miralles, D. G.; Martens, B.; de Roo, A. MSWEP: 3-Hourly 0.25° Global Gridded Precipitation (1979–2015) by Merging Gauge, Satellite, and Reanalysis Data. *Hydrol. Earth Syst. Sci.* **2017**, *21* (1), 589–615. https://doi.org/10.5194/hess-21-589-2017
50. Bao, X.; Zhang, F. Evaluation of NCEP–CFSR, NCEP–NCAR, ERA-Interim, and ERA-40 Reanalysis Datasets against Independent Sounding Observations over the Tibetan Plateau. *Journal of Climate* **2013**, *26* (1), 206–214. https://doi.org/10.1175/JCLI-D-12-00056.1
51. Sharp, E.; Dodds, P.; Barrett, M.; Spataru, C. Evaluating the Accuracy of CFSR Reanalysis Hourly Wind Speed Forecasts for the UK, Using in Situ Measurements and Geographical Information. *Renewable Energy* **2015**, *77*, 527–538. https://doi.org/10.1016/j.renene.2014.12.025
52. Tian, W. Evaluation of Six Precipitation Products in the Mekong River Basin. *Atmospheric Research* **2021**, 13
53. Lu, X. X.; Li, S.; Kummu, M.; Padawangi, R.; Wang, J. J. Observed Changes in the Water Flow at Chiang Saen in the Lower Mekong: Impacts of Chinese Dams? *Quaternary International* **2014**, *336*, 145–157. https://doi.org/10.1016/j.quaint.2014.02.006.